Experimental cell with a Fabry-Perot resonator tuned in situ for magnetic resonance studies of matrix-isolated radicals at temperatures below 1 K

S. Sheludiakov,[1] D. M. Lee,[1] V. V. Khmelenko,[1] J. Järvinen,[2] J. Ahokas,[2] and S. Vasiliev[2]
[1)] *Institute for Quantum Science and Engineering, Department of Physics and Astronomy, Texas A&M University, College Station, TX, 77843, USA*[a)]
[2)] *Department of Physics and Astronomy, University of Turku, 20014 Turku, Finland*

(Dated: 23 May 2020)

We describe the design and construction of an experimental cell for the study of free radicals in macroscopically thick films of solidified molecular and rare gases by 128 GHz Electron Spin Resonance (ESR) at temperatures below 1 K. The ESR resonator has an open Fabry-Perot design and its frequency can be tuned *in situ* by adjusting the spacing between the mirrors. The tuning mechanism consists of a piezo positioner and stainless-steel edge-welded bellows which can change the resonator frequency by at least 6 GHz. The films of solidified gases can be deposited either directly from a room temperature reservoir or by recondensing from a specially arranged chamber. The free radicals can be created in the solid films by dissociating matrix species by running an rf discharge in helium vapor. We suggest that such a sample cell design can also be used for a broad range of low-temperature ESR experiments where sample cooling needs to be enhanced by the presence of superfluid helium.

I. INTRODUCTION

Electron spin resonance (ESR) is one of the most versatile and convenient techniques for probing dynamics of species with unpaired electron spins. Modern ESR techniques allow conducting measurements in high magnetic fields of several tesla and at high frequencies which can even enter the terahertz range[1,2]. The characteristic features of such experiments involve the use of quasi-optical techniques and open-design Fabry-Perot resonators[3,4]. In contrast to the UV and visible-range optical methods, mm-wave photons have energies of order μeV which makes ESR spectroscopy particularly attractive for measurements below 1 K. The low-temperature measurements, however, require tackling the problems of thermal contact between the sample and environment, long relaxation times to thermal equilibrium, and a possible shift of the ESR resonator frequency upon cooling due to thermal contraction or a change of the sample properties. The cavity resonance frequency is defined by the resonator physical dimensions and can rarely be adjusted *in situ* at low temperatures. One of the practical possibilities to adjust the resonator frequency would be to use a system of differential screws with a stepper motor or manual rotator which, however, lack precision and reliability. Currently available piezo positioners, however, become a viable low-temperature alternative with an unmatched level of precision. They can be employed for tuning the resonance frequency of Fabry-Perot cavities[5], adjusting the frequency of planar microresonators[6], or performing sample rotation with a required orientation in an external static magnetic field[7]. Driving a piezo crystal, however, leads to inevitable heat dissipation which requires special attention to cooling of the positioner.

The samples created at low temperatures, such as solidified films of molecular and rare gases containing stabilized free radicals, *e.g.* for polarized target research[8], represent one of the examples where the *in situ* adjustment of resonance frequency is highly desirable. In this case, thick samples alter the effective dielectric constant, ε, of the cavity and shift the cavity resonance frequency, $f \sim 1/\sqrt{\varepsilon}$. In our previous work, we designed and used a sample cell for ESR studies of H atoms in thin solid films of molecular hydrogen isotopes at temperatures below 1 K[9]. The sample chamber accommodated an ESR semiconfocal Fabry-Perot resonator operating at f=128 GHz with its lower mirror serving as the top electrode of the quartz microbalance. Such an arrangement allowed us to estimate the H_2 film deposition rate and thickness using the microbalance and to probe the signal of H atoms embedded in the film by ESR. However, a limited operating range (f=128.5 $\pm$0.5 GHz) of our ESR spectrometer constrained the H_2 film thicknesses to about 200 μm, while thicker H_2 films would shift the resonator frequency outside the spectrometer operation range.

In this work, we present the design and performance of an experimental cell for carrying out ESR studies of stabilized atoms in macroscopically (of order 1 mm) thick molecular films using 128 GHz ESR spectroscopy in a high magnetic field of 4.6 T and at temperatures below 1 K. Unlike the earlier design, the quartz microbalance is arranged as the sample cell bottom which also allows using both bulk solid molecular or rare-gas films as well as superfluid helium as the hosting medium to stabilize free radicals. The present sample cell design allows an *in situ* adjustment of the ESR resonator frequency within at least 6 GHz using a combination of a stainless steel edge-welded bellows and a piezo positioner. Similar to the earlier design, the solid molecular or rare-gas films can be created with monolayer precision and an adjustable deposition rate. We suggest that our sample cell design can be used for low-temperature ESR experiments with a variety of free radicals especially in cases of their very small concentration when having large sample volumes becomes beneficial. In particular, this sample cell can be adapted for the studies of free radicals in loose networks of solid molecular and rare-gas strands created inside bulk superfluid helium, so-

[a)] Electronic mail: seshel@physics.tamu.edu

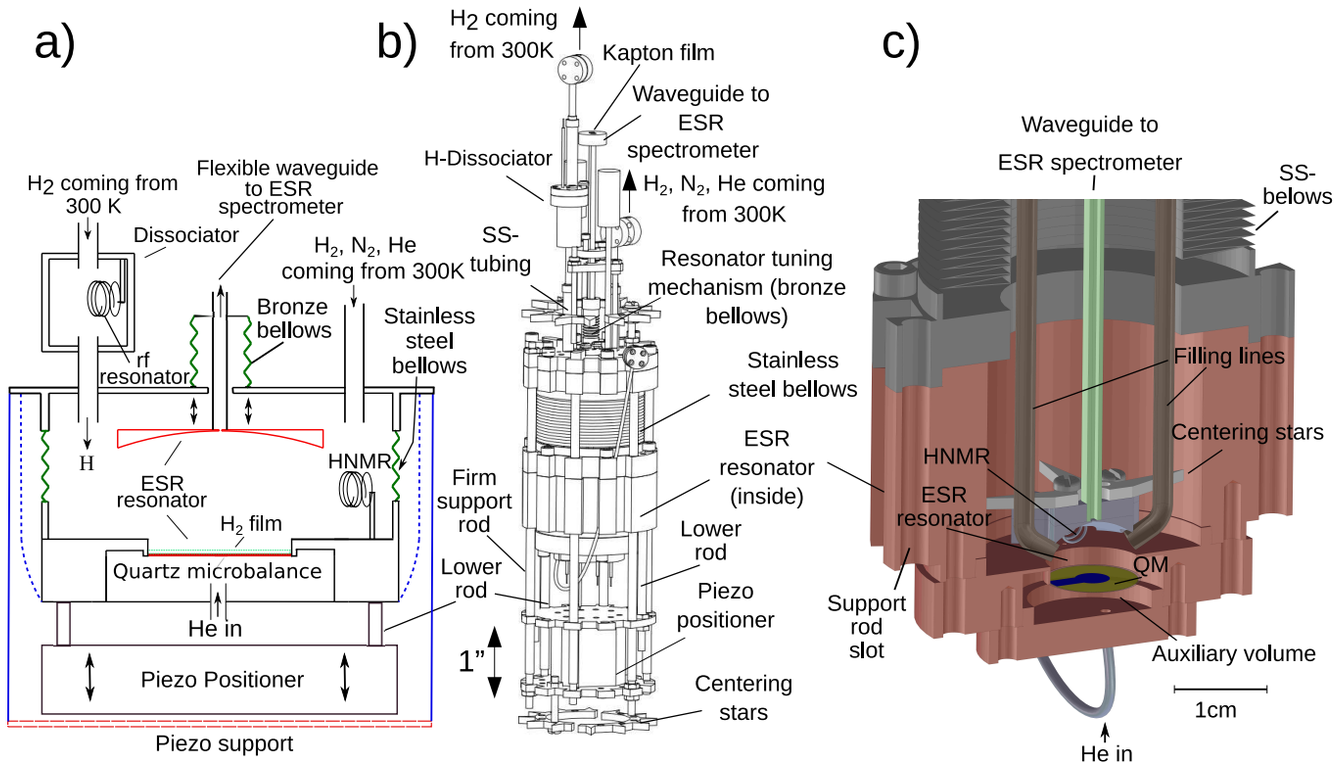

FIG. 1. a) Sample cell simplified schematic. Firm support rods and flexible thermal links between the flanges are schematically presented by blue solid and dashed lines, respectively. (b) Actual sample cell, and c) ESR resonator model. The top gold QM electrode is shown as semi-transparent. The bottom key-hole shaped gold electrode is shown in blue for convenience.

called impurity-helium condensates[10,11]. Finally, the current sample cell design can be employed for a broad range of studies where the thermal contact between the sample and environment must be enhanced by the presence of a helium exchange gas or superfluid ^{4}He film.

II. SAMPLE CELL

The experiments for studying H and N atoms in solid H_2 and N_2 films are carried out in the sample cell (SC) shown schematically in Fig. 1a and as a full-size model in Fig. 1b. The SC provides an opportunity to study samples of H and N atoms as well as other free radicals in solid H_2, N_2, and other molecular and rare-gas matrices using two quantitative techniques: 128 GHz ESR spectroscopy of free radicals and the solid film mass measurement by a quartz microbalance. The host solid films are deposited onto a flat mirror of the ESR resonator which also serves as a top electrode of the quartz microbalance. The sample cell allows a two-stage tuning of the ESR resonator frequency: a coarse frequency adjustment at room temperature (RT) using a miniature bronze bellows and a set of screws as well as *in situ* fine tuning of the cavity frequency for low temperatures, using a system of stainless steel bellows and a piezo positioner. From now on, we will mainly discuss the sample cell construction in the light of our studies of H atoms in solid H_2 films, but all methods and conclusions can also be applied for a variety of free radicals in different solid molecular and rare-gas matrices.

The SC consists of a main volume (Fig. 1c) which accommodates a semiconfocal 128 GHz ESR Fabry-Perot (FP) resonator and a 910 MHz NMR helical resonator (HNMR), as well as an auxiliary (bottom) volume under the quartz microbalance. The H-dissociator, a chamber where we condense H_2 gas used later for the H_2 film deposition and production of a flux of gas-phase atomic hydrogen (Fig. 1b), is arranged about 4 cm above the main SC volume. The ESR resonator is coupled to a 128 GHz ESR spectrometer attached to the 1K pot of the dilution refrigerator[4] via an assembly of copper and copper-nickel waveguide sections. The waveguide flange is sealed with a Kapton film (Fig. 1b) glued along its perimeter to keep the main sample cell volume vacuum tight. The HNMR coil is used to run an rf discharge in helium vapor and to create H atoms in the H_2 film as well as to initiate an NMR transition of hydrogen atoms in the H_2 film.

The SC is attached to the mixing chamber of an Oxford 200 dilution refrigerator and also located in the center of a 4.6 T superconducting magnet with a homogeneity $\Delta B/B$=10^{-6} in 1 cm^3. The SC assembly consists of four flanges machined from oxygen-free high thermal conductivity (OFHC) copper and stainless steel bellows sealed with indium gaskets all bolted together. The sample cell is attached to the mixing chamber by three 0.1875" 8-inch long annealed OFHC rods. This allows us to cool down and stabilize the sample cell

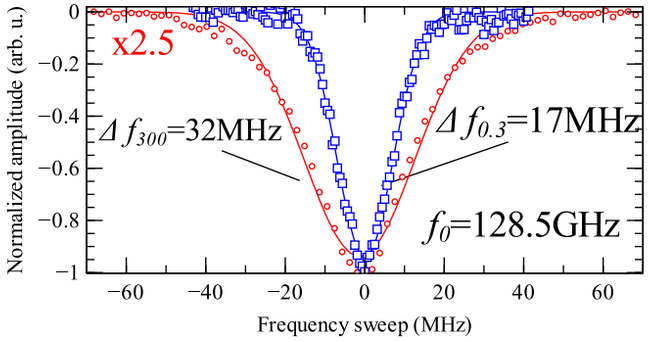

FIG. 2. ESR resonator curves measured at 300 K (red circles) and 0.3 K (blue squares). Fits of experimental data by Gaussian curves are shown by red and blue solid lines, respectively. The resonator curve amplitudes were normalized for convenience. For the purpose of comparison the signal measured at T=300 K was multiplied by a factor of 2.5.

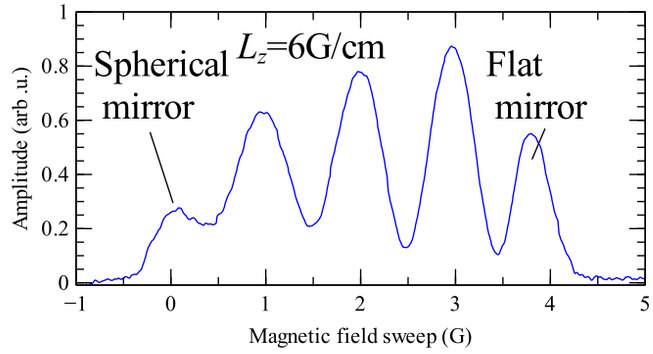

FIG. 3. ESR signal of H atoms in the gas phase measured in axial, L_z, gradient 6G/cm. Each peak corresponds to the antinode of the mm-wave magnetic field in the Fabry-Perot cavity. The antinodes at the surface of semi-spherical and flat mirror are the most left and right ones, respectively. The ESR resonator is tuned to the TEM_{004} mode.

temperature during the experiments in the range 0.13-1 K. In order to provide proper cooling to the sample substrate and minimize the temperature difference between the copper flanges separated by the stainless-steel bellows, we used three 4-inch long 0.125" OFHC copper rods with 2-inch long *flexible* copper braids brazed to their ends as shown schematically by dashed blue lines in Fig. 1a. This made a strong enough thermal link between the flanges and allowed moving the lower flanges by the piezo positioner. The temperature difference between the flanges was about 5-10 mK at T=0.13 K when no superfluid He film was present in the sample cell. The SC alignment with respect to the axis of the dilution refrigerator is made with two sets of Teflon star spacers installed on the sample cell top and bottom flanges.

The bottom of the positioner is bolted to a copper plate which is also firmly attached to the top sample cell flange by three 0.125" 4-inch long OFHC copper rods passing through the slots in the bellows and lower copper flange (see Fig. 1c) without friction. The top movable platform of the piezo positioner is attached to a copper plate which is bolted to the copper flange below the bellows by two 2-inch long 0.125" OFHC copper rods indicated as lower rods in Fig. 1b. Such an arrangement allows moving the flat ESR mirror relatively to the top copper flange and upper semi-spherical mirror, thus performing tuning of the resonance frequency.

A. ESR resonator

In the present sample cell construction we employed a semiconfocal Fabry-Perot resonator, a design we used in our previous ESR studies of H atoms in solid H_2 films[9,12–14], H atoms in the gas phase[15], and also of silicon doped with phosphorus and arsenic[5]. The resonator has an open design which allows arranging auxiliary probes and gas condensing lines close to the sample without distorting the mm-wave magnetic field in the cavity. The upper semi-spherical resonator mirror with a diameter d =9.7 mm and an aperture of 18 mm is made of silver-plated OFHC copper. A 0.5 mm hole in the mirror center is used to couple the cavity to the waveguide. The H_2 and He filling lines (Fig. 1c) are aligned inside the sample cell using Teflon spacers to avoid thermal contact with the resonator mirror. The top resonator mirror is also centered inside the sample cell with a set of Teflon spacer stars. The bottom flat mirror also serves as a top 400 nm thick gold electrode which covers nearly the whole surface (d=9 mm) of the quartz disc (d =10.5 mm). This is much greater than the diameter of the mm-wave field antinode ($\simeq$3 mm) near the QM surface which ensures low radiation losses in the resonator. We chose the electrode thickness to be significantly greater than the mm-wave skin depth in our experimental conditions ($\leq$100 nm) and thin enough to ensure that the QM response during the film deposition is still linear. The unloaded ESR resonator has a resonance linewidth of 32 MHz at T=300 K and 17 MHz at T=0.3 K and the Q-factors of $\simeq$4000 and 7500, respectively (Fig. 2), which are comparable to those in our previous designs. The oscillating, H_1, magnetic field in the resonator can typically be varied from $\sim$1 μG (applying power $\sim$1 pW) while sweeping through the ESR lines up to $\sim$1 mG ($\sim$1 μW) for the Dynamic Nuclear Polarization (DNP) experiments[14,16]. Applying the maximum mm-wave field power in the resonator slightly overheats the sample cell as can be detected directly at the lowest temperatures. This also allows us to measure the power and amplitude of the mm-wave field in the cavity by a comparison with heating the SC to the same temperature using an electrical heater.

A distribution of the mm-wave field in the Fabry-Perot cavity tuned to the TEM_{004} mode used in our studies[13] can be visualized by an ESR signal of gas-phase H atoms taken in an applied axial magnetic field gradient (Fig. 3). The H gas fills the whole volume between the mirrors and the H atom ESR line maxima directly correspond to the mm-wave field antinodes of the FP cavity.

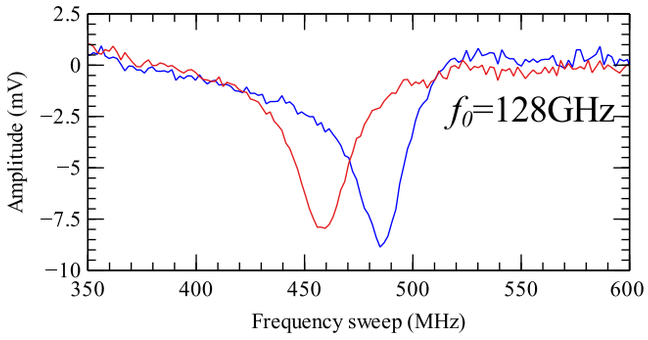

FIG. 4. ESR resonator curves before (red line) and after moving the bottom mirror up by a single piezo positioner step applying V=70 V (blue line).

B. Resonator tuning mechanism

In order to study thick H_2 films, we designed a two-stage tuning system which would compensate the ESR cavity shift after the H_2 film deposition. Condensation of a 1 mm H_2 film (ε_{H_2}=1.28) would decrease the ESR resonator frequency by about 2.5 GHz. The compensation of the cavity frequency shift is of crucial importance due to the limited operating range of our ESR spectrometer (128.5±0.5 GHz) defined by the mm-wave bandpass filter[4]. Adjustment of the ESR cavity frequency is done in two stages. First, we perform coarse cavity tuning at room temperature before closing the vacuum can using a system of screws and upper miniature bronze bellows[9]. The waveguide with the semi-spherical mirror is soldered to these upper bellows and by squeezing or extending them, the upper mirror can be moved up and down by ≃1 mm. It is important that the 30 cm long waveguide section coming from the ESR spectrometer is flexible enough to allow such an adjustment. This is sufficient to set the cavity frequency within a range of several GHz in the vicinity of a proper mode for operation. We typically work at the TEM_{004} mode which corresponds to a mirror separation of 6.7 mm. The cavity fine tuning is organized by a combination of lower soft edge-welded bellows and a piezo positioner which is able to move the bottom flat mirror within a distance of order 1 mm with a desired accuracy. The piezo positioner can be used in either a step or a continuous mode. The former regime makes it possible to displace the bottom flat mirror by a single slip-stick driving step. The latter regime implies driving the positioner in multiple steps with a repetition frequency up to 10 kHz. A typical ESR resonator frequency shift by applying a maximum single driving step of 70 V to the positioner is shown in Fig. 4. The resonator frequency change (25 MHz) corresponds to the positioner displacement by 1.1 μm. The displacement steps can be decreased by choosing a smaller driving voltage.

The edge-welded bellows implemented for the fine tuning are made of austenitic 316L stainless steel. They were purchased from the UHV-design company[17]. Being the softest in their class they also possess a vanishingly small residual magnetization. The latter factor is particularly important for magnetic resonance experiments. The inner and outer bellows diameters are 21 and 39 mm, respectively. The bellows consist of 16 convolutions with a spring constant of 49 N/m per convolution and custom made stainless flanges (see Fig. 1b). In order to change the position of the bottom mirror, we used a titanium ANPz101/LT piezo positioner purchased from Attocube systems[18]. The positioner model is rated for lifting 100 g with a maximum dynamic force 5 N. From the CAD design we estimated that the total mass of the sample cell and bellows flanges to be lifted by the piezo positioner is ≃320 g. Due to a rather large mass of the sample cell parts to be moved, we expected that the piezo driving steps for the bottom mirror displacement when moved up and down could be markedly different. In order to tackle this, we adjusted the stainless steel bellows to be slightly extended from their equilibrium length, so they acted as a spring and the Hooke's force they exerted somewhat compensated for the weight of the sample cell parts to be displaced. It turned out, that by varying the stainless steel bellows extension within about 1-1.5 mm, we were able to clearly see the difference in the ESR cavity frequency change while stepping the piezo (and moving the bottom ESR mirror) up and down. The steps up for the smallest bellows extension were 30-50% smaller as compared with the steps down. The steps up for the largest bellows extension were about 10% *larger* than the steps down while using the same piezo driving voltage. We also paid special attention to the rigidity of cables and capillaries coming to the sample cell which may impede the tuning. We used flexible CuNi coaxial cables in a Nb-Ti shield and the stainless-steel capillaries were bent into a spiral.

After the coarse tuning is made, we closed the vacuum can of the dilution refrigerator and started pumping the sample cell and vacuum can volumes through the needle valve. We also observed that the piezo positioner was not able to sustain a differential pressure between the bellows walls (inside and outside the bellows) above ≃10 mbar. A higher differential pressure contracts them if the pressure outside the bellows is higher than that inside the sample cell volume or extends them otherwise, thus resulting in a cavity frequency shift. Therefore, we made a preliminary cavity tuning at room temperature keeping one atmosphere of air or dry nitrogen gas in the sample cell volumes. In this case, no differential pressure is built up. Evacuating the cell to high vacuum increased the resonance frequency by about 1 GHz. Cooling the sample cell to 77 K also increased the frequency by extra 300 MHz. Cooling it further down to 4.2K shifted the cavity frequency up by another 100 MHz.

We also observed that accurate centering of the sample cell inside the vacuum can is important for performing fine tuning of the resonator. Proper sample cell alignment increased the value of the bottom mirror displacement while stepping up by about 20-30%. In case of misalignment, the piezo positioner may also become stuck while cooling down to about 77 K. This can be overcome by creating a small, 15 mbar, differential pressure by adding helium gas into the vacuum can volume. This extra pressure compensates for friction caused by the cell misalignment and helps the positioner lift the flange with the flat ESR mirror.

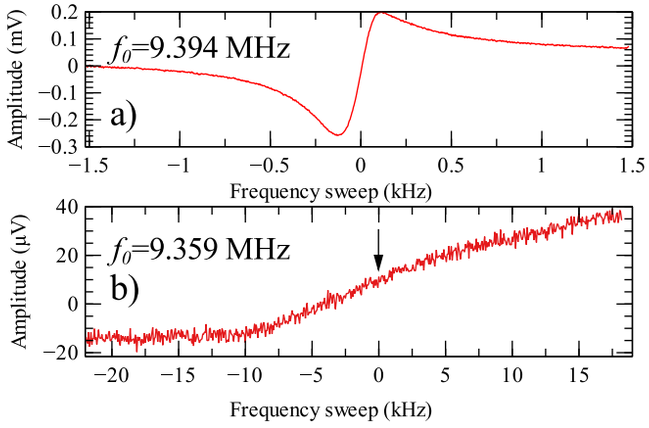

FIG. 5. a) Quartz microbalance resonance curve measured after the deposition of a 3 μm thick H_2 solid film and b) Deterioration of the QM resonance curve after depositing a 20 μm thick H_2 film. The expected QM resonance frequency position based on the deposition time is shown by the arrow. Note the difference in shapes and amplitudes of the QM curves.

We paid special attention to estimate the heat release while driving the piezo positioner which is particularly important at low temperatures. A single driving step with a maximum driving amplitude V=70 V did not produce any noticeable, within about 1 mK, SC heating at T=0.15 K. We did not observe any sample cell heating while driving the positioner by 100 steps with a repetition rate of 1 Hz. Driving a positioner with 150 Hz repetition rate for about 0.5 s at the same driving amplitude overheated the sample cell from 0.15 to about 0.3 K.

We also carefully studied the tuning system performance in high magnetic field. The bellows are located in a homogeneous static magnetic field with a vanishingly small gradient and zero dragging force. As a result, we did not observe any difference in the performance of the fine tuning system in a zero or in a high (4.6 T) magnetic field.

C. Quartz microbalance

The microbalance was made using an AT-cut quartz single crystal disc purchased from Krystaly Hradec Kralove a.s. (Czech Republic)[19]. The disc was polished from both sides; it had a diameter of 10.5 mm, thickness of 0.166 mm, and a fundamental oscillation frequency of f_0=10 MHz. Prior to sputtering 400 nm thick gold electrodes, we predeposited 15 nm thick copper layers onto the quartz to improve the adhesion of gold. We avoided depositing magnetic chromium or nickel layers typically used for this purpose in order to keep from destroying the magnetic field homogeneity required for high-resolution ESR measurement. The top QM electrode is round and covers nearly the whole quartz disc surface (d=9 mm). The bottom electrode has a key-hole shape with a diameter 3.8 mm (Fig. 1c)[9]. The copper QM leads are glued near the disc edge using conducting epoxy. Sputtering the electrodes and gluing the leads decreased the QM fundamental frequency down to 9.4 MHz. However, the QM behavior was still linear during the deposition of rather thin, of order 1 μm H_2 films. The quartz microbalance in the present design is arranged as the lowest place in the sample cell. This gives an opportunity to collect macroscopic amounts of H_2 and superfluid helium in the cavity. The QM is glued directly along its perimeter to the copper flange by Stycast 1266 epoxy without a Stycast 1266 spacer used in the previous SC construction[9]. We took special care to avoid breaking the QM upon cooling due to differential contraction of copper and quartz. The copper flange thickness at the place of gluing was reduced to 0.2 mm.

We also arranged an auxiliary volume below the QM (see Fig. 1c) where a small, ∼mmol, amount of He is condensed prior to the H_2 film deposition. The superfluid helium film flushes the QM surface and removes heat released during the sample deposition and recombination of H atoms in the H_2 film.

The QM resonance curve at T=0.13 K has a width of 280 Hz and the Q-factor of $3\cdot10^4$. The QM operates in a reflection mode and its frequency was detected using a reflection measurement with a frequency-modulated rf excitation. The rf stimulus is sent to the QM through a directional coupler, so the reflected signal is then collected by a detector which outputs DC voltage proportional to the incoming rf power. The frequency deviation, 40 Hz, was chosen to be significantly smaller than the QM resonance curve width (Figs. 5a and b) in order not to produce any substantial broadening. The long-term (over 5 hours) QM frequency stability at the fundamental frequency was 2 Hz which corresponds to the detection accuracy of three H_2 monolayers.

D. Film deposition

The new sample cell allows us to create films of solid molecular hydrogen using two different approaches: by quench-condensing H_2 onto the QM surface from a room temperature gas-handling system or by depositing it at lower temperatures from a specially arranged chamber (H-dissociator) thermally insulated from the SC body by stainless steel tubing (Fig. 1c). In order to condense H_2 directly from a RT reservoir, we heated the filling line up to 15-20 K (above the H_2 triple point) using electrical heaters placed along the tubing while keeping the sample cell cold, $T \simeq$1 K. After entering the SC, the condensing lines are directed toward the center of the QM as shown in Fig. 1c. Cold H_2 molecules reaching the SC hit the QM surface and freeze instantaneously. As a result, they do not have enough energy to diffuse and aggregate into equilibrium bulk polycrystallites which tend to form due to incomplete wetting of metallic substrates by H_2 below the triple point[20,21]. The condensing lines are long enough which ensures that the H_2 molecules are well thermalized when they enter the sample cell. In case of the direct deposition of H_2 films from the RT gas-handling system, we control the deposition rate by adjusting the condensing pressure with a needle valve.

The second possibility is to deposit H_2 films using the gas

which was loaded into the H-dissociator chamber in advance. For this purpose, we condense there of order a few tenths of mmol of H_2 gas; the loading process can also be controlled by the H-dissociator rf helical resonator frequency change due to the accumulated solid H_2 layers (Fig. 1a). Condensing 0.1 mmol of H_2 decreases the rf resonator frequency by about 0.5 MHz. The H-dissociator has a weak thermal link to the continuous heat exchanger of the dilution refrigerator. The film deposition from the H-dissociator chamber is carried out by heating it from $\simeq$0.3 K to temperatures of 5-6 K where the H_2 vapor pressure becomes sufficiently high to start building up the film on the QM surface. The deposition rate in this case can be accurately adjusted in a range 0.01-10 monolayers per second by regulating the chamber temperature[9]. This deposition method is particularly convenient for depositing thin H_2 films where a precise deposition control is required. The sublimated H_2 molecules (T=5-6 K) are even colder than in the case of direct deposition (T=15-20 K) which should lead to more uniform solid hydrogen films grown on the surfaces of the Fabry-Perot cavity mirrors.

The H-dissociator chamber also contains a separate helical resonator (f=750 MHz) which we use to create a flux of atomic hydrogen gas into the SC by running the rf discharge there. The ESR lines of these gas-phase H atoms provide a magnetic field reference for determining the g-factor of H atoms in the H_2 matrix and evaluating concentration-dependent shifts of the ESR lines of H atoms in the H_2 films as well as the local H atom concentrations in the solid matrix[13].

The QM performance degraded significantly during deposition of thick H_2 films. The QM Q-factor and resonator coupling decreases for thicker films which makes detection of the QM frequency much less accurate. The QM resonance curve deterioration after depositing a 20 μm H_2 film is shown in Fig. 5b. Therefore, in order to deposit H_2 films thicker than $\sim$20 μm we stabilized the H_2 gas flow in the beginning of deposition when the QM is highly sensitive and estimated the film thickness based on the deposition time. The deposition of thick H_2 films also decreases the ESR resonator frequency. This can also be used for a coarse, of order ten μm, estimate of the H_2 film thickness.

The present sample cell design also makes it possible to condense other molecular and rare-gas solid matrices. To demonstrate this possibility, we performed accumulation of an N_2 film. In this case, the sample cell is kept at a temperature of 5-10 K where the nitrogen vapor pressure is essentially zero. The N_2 gas is condensed directly from a room temperature reservoir while the condensing line is heated above T=77 K by electrical heaters. In this case, the temperature along the condensing line is determined by three platinum resistance thermometers.

E. NMR resonator

In this sample cell design we also arranged an auxiliary helical resonator (HNMR in Fig. 1) in the vicinity of the QM. This resonator was used for NMR measurements of H atoms as well as for running the rf discharge in a helium

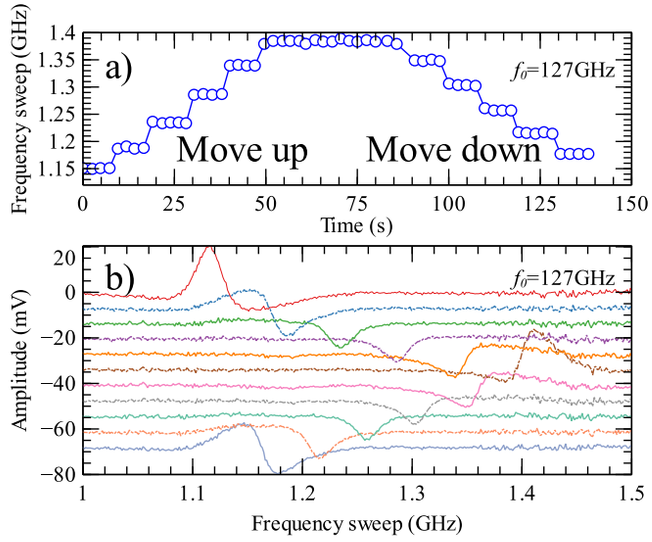

FIG. 6. a) ESR resonator frequency change after five steps of moving the bottom mirror using piezo positioner up and down. b) Amplitude of the resonance curves of the ESR cavity in the absence of the sample shown by different colors for each piezo displacement step shown in (a). The resonance positions were considered to occur at the curve minima. Note that the frequency change for moving the bottom ESR resonator mirror up is larger than while moving it down using the same conditions for driving the piezo positioner.

vapor and dissociating a fraction of the H_2 molecules in the solid H_2 films. We tuned this resonator to f=910 MHz in order to match the H atom NMR transition frequency in our magnetic field of 4.6 T. The resonator is coupled to a coaxial line with a coupling loop and grounded at one end. In this configuration, the electric and magnetic field maxima are close to the open and grounded ends of the helical resonator, respectively. The resonator frequency is defined by the length of the wire it is made of ($d \simeq \lambda/4$) and can also be fine-tuned at room temperature by adjusting the spacing between the coil windings corresponding to the distributed capacitance.

Even though the film is located outside the HNMR coil, the NMR transition for H atoms in a solid H_2 film can be excited by the helical resonator fringing field. In our studies, we detect the NMR transition indirectly. We sweep an rf excitation in the vicinity of NMR transition frequency and detect a change of the H atom ESR line amplitude when the rf excitation passes though the resonance[9]. Typically, the excitation powers of order a few tens of μW suffice.

The helical resonator was also used to run the discharge in the helium vapor to produce H atoms in the solid molecular hydrogen films. The discharge is run by sending rf pulses of order a few watts to the HNMR coil with a typical pulse duration of 0.1 ms and duty cycle of 1/200. The electrons created during the discharge have energies of order 100 eV and can dissociate H_2 molecules in a solid hydrogen film to within a depth $\simeq$80 nm[9].

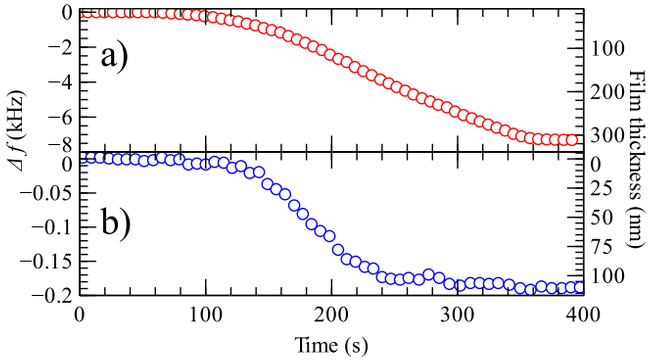

FIG. 7. a) Quartz microbalance frequency change during deposition of a 340 nm solid N_2 film. b) QM frequency change during deposition of a 110 nm H_2 film on top of the existing N_2 film.

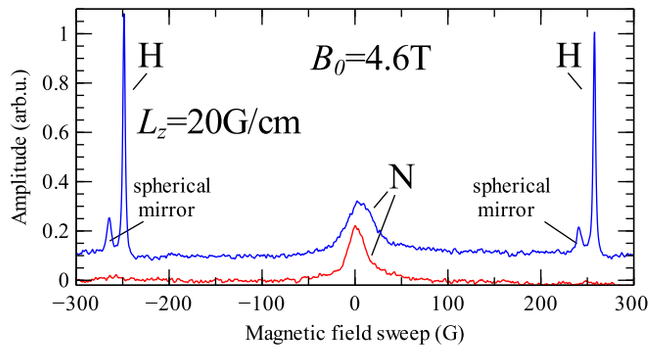

FIG. 8. ESR spectra of N atoms in a 340 nm solid N_2 film (red line) and after adding a 100 nm solid H_2 film with embedded H atoms on top of the existing N_2 film (blue line) both measured at T=0.6 K in the applied axial magnetic field gradient L_z=20G/cm . The smaller H atom line components are the contribution from H atoms in the H_2 films formed on the upper semi-spherical mirror.

III. SAMPLE CELL PERFORMANCE

After the sample cell was assembled, installed, and checked for leaks, we carried out two preliminary experimental runs in order to test the sample cell performance. First, we present the performance of the tuning mechanism for adjusting the ESR resonator frequency. The preliminary test of the tuning system operation was carried out at room temperature and having one atmosphere of air in the sample cell. For that purpose, we adjusted the stainless steel bellows to be slightly extended from their equilibrium length. After that we applied five steps to the piezo positioner (V=70 V) with a 10 s delay after each step to move it first up then down (Fig. 6a). The bottom mirror displacement in these conditions was larger while moving it up, so the final ESR cavity frequency after driving the piezo five steps up and down was larger than that before starting this test. The resonator frequency after each step up and down changed by ≃60 and 50 MHz, respectively. The changes of the position of ESR cavity resonance during these operations are shown in Fig. 6b. The amplitudes of the resonance curves of the FP cavity changed their shape which made a precise determination of the resonance frequency ambiguous. In this preliminary test, we considered that the cavity resonance frequency corresponds to the resonance curve minima. We also observed that the ESR resonator frequency in these conditions can be changed within at least 6 GHz by moving the bottom mirror. This should be sufficient to compensate for the resonator frequency shift after the deposition of a 2.8 mm thick solid H_2 or a 1.8 mm thick solid N_2 film (ε_{N_2}=1.52).

After that we extended our evaluation of the sample cell performance to preliminary ESR experiments. A typical experimental procedure consisted of closing the setup, consecutive cooling to 77 K, 4.2 K, and then to temperatures below 1 K by starting the dilution refrigerator. For our preliminary sample cell tests we tried deposition of two solid films with markedly different melting temperatures: solid hydrogen (T_m=14 K) and nitrogen (T_m=63 K). The solid H_2 films can be deposited by keeping the sample cell at T=0.7-1.5 K, and between 4.2-10 K for the molecular nitrogen films. In this preliminary run, the N_2 film was deposited before starting the dilution refrigerator, while the initial SC cooling to 4.2 K was made using helium exchange gas. However, the sample cell design also allows depositing solid N_2 while operating the dilution unit as a ^{4}He or ^{3}He refrigerator. First, we deposited a 340 nm solid N_2 film on the QM surface directly from a room temperature reservoir. The QM frequency change during this deposition is presented by open red circles in Fig. 7a. After that we condensed a few μm of He into the SC and started the rf discharge in order to accumulate N atoms in solid N_2. We did not observe an expected triplet of nitrogen atom ESR lines separated by ≃4.2 G due to the hyperfine interaction[22] but rather a single broad line with a width ≃25 G (Fig. 8). The ESR line area is proportional to the number of N atoms in the film. The linewidth, however, is mainly determined by the dipolar interaction between the N atom electron spins which smears out the N atom triplet and also provides information on the local N atom concentration. An ESR spectrum of N atoms in solid N_2 in the end of N atom accumulation when the signal stopped increasing and the local N atom concentrations approached ≃4×10^{19}cm^{-3} is shown in Fig. 8 by a solid red line. The time evolution of the N atom line area in the course of running the discharge is presented in Fig. 9 by open red circles. We were unable to retrieve the N atom signal reliably at the beginning of accumulation due to the presence of a broad cyclotron resonance line of free electrons in the discharge zone which overlapped with the N atom ESR line.

In this preliminary run, we were also able to cool the sample of N atoms in solid N_2 down to temperatures of about 0.16 K, the lowest temperature the N atoms were ever stabilized at. We did not observe any influence of temperature on the shape of N atom ESR spectra in this temperature range. As a future possibility, reaching higher N atom concentrations stabilized in solid N_2 may also lead to the appearance of exchange effects or collective magnetic phenomena which may emerge upon cooling the system to even lower temperatures.

At the next stage, we evacuated the helium film from the sample cell and deposited a 110 nm H_2 film on top of the

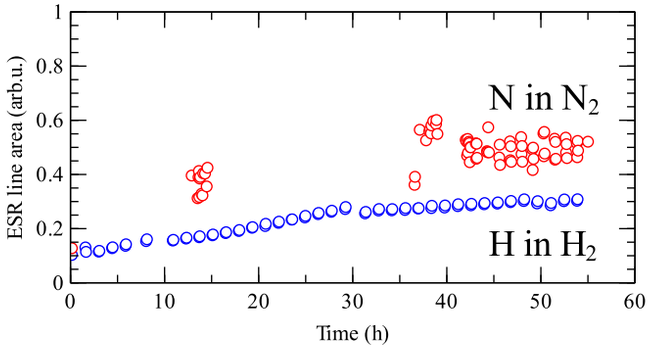

FIG. 9. Evolution of ESR signal of N atoms in a 340 nm solid N_2 film and H atoms in 110 nm H_2 film deposited on top of it as a function of accumulation time.

existing solid N_2 film. For that purpose we used the second, more accurate approach: the H_2 molecules were recondensed onto the QM surface from the H-dissociator where the H_2 gas was solidified in advance. The graph of QM frequency change during the H_2 film deposition is presented in Fig. 7b. After that we condensed a few μmol of He into the sample cell and started the rf discharge again.

The H atoms formed a well resolved doublet of ESR lines each with a width of 1.5 G and separated by 507 G. During the film deposition, the H_2 film also partially accumulated on the upper semi-spherical mirror. This resulted in the second broader and much smaller signal corresponding to H atoms accumulated there. The ESR spectrum presented in Fig. 8 was measured by applying an axial magnetic field gradient L_z=20 G/cm. A much greater linewidth of N atoms makes it impossible to resolve the possible contribution from N atoms in solid N_2 deposited on the spherical mirror. Evolution of the H atom ESR line areas during the course of running the discharge is presented in Fig. 9 by blue circles. By running the discharge we achieved a local concentration of H atoms in solid H_2 of order 1×10^{19}cm^{-3}. Unlike N atoms in solid N_2, the H atoms in solid H_2 remain highly mobile during the discharge and can recombine back to molecules. This leads to much smaller H atom concentrations in the end of an accumulation process as compared with that of N in solid N_2. An ESR spectrum of H atoms in a 110 nm solid H_2 film and N atoms in the underlying 340 nm N_2 film is shown in Fig. 8 by a solid blue line.

The larger mass and binding energy of N_2 molecules as compared with those of H_2, 9.8 and 4.5 eV, respectively, also resulted in remarkably different penetration depths of electrons from the discharge into the solid films. The probability for a direct dissociation of H_2 and N_2 molecules inside the films by electron impact decays exponentially with distance x from the film surface, $\sim\exp(-x/d)$, where d is the characteristic penetration depths of electrons into solid H_2 or N_2. If we consider that the H_2 and N_2 film surface areas are equal, 63% of H and N atoms should reside within the surface layers equal to electron penetration depths d for solid H_2 and N_2, respectively. As a majority, these shallow atoms also provide the main contribution to the ESR linewidth. The values of d for solid H_2 and N_2, therefore, should follow the ratio of N/n, where N is the number of H and N atoms and n is their average local concentration, respectively. Due to a larger electronic spin, S_N=3/2, as compared with S_H=1/2, the N atom ESR linewidth is enhanced by a factor $[S_N(S_N+1)]/[S_H(S_H+1)]$=5 (Ref. [23]). The line areas in our conditions of low temperatures and high magnetic field have the scaling factor of 3 from the ratio of N and H atom electron spins[24].

The H:N line area ratio gives the total number of N atoms in the N_2 film to be about 0.6 of that of H atoms in the H_2 film. From the linewidth, the local N atom concentration, however, exceeds that of H atoms by a factor of about three. Therefore, we estimate the penetration depth of $\sim$100 eV electrons into solid N_2 to be $\simeq$15 nm as compared with about $\simeq$80 nm into the solid H_2 films measured in our previous study[9]. As a continuation of this preliminary work, we plan to utilize this newly built sample cell for the studies of spatial quantum diffusion of H atoms in macroscopically thick solid H_2 films and free radicals in impurity-helium condensates.

In conclusion, we presented the design and performance of a new versatile sample cell for the ESR studies of free radicals in solid matrices at temperatures below 1 K. The sample cell allows us to carry out an *in situ* adjustment of the ESR resonator frequency by the tuning mechanism based on a piezo positioner and edge-welded stainless steel bellows. We demonstrated the performance of this sample cell by a registration of H atoms in solid H_2 films and N atoms in solid N_2 films at T<1 K. We suggest that such a design can be implemented for a broad range of low-temperature ESR experiments with a variety of free radicals or studies where the thermal contact between the sample and environment is required to be enhanced by the presence of a helium exchange gas or superfluid ^{4}He film.

ACKNOWLEDGMENTS

This work has been supported by NSF Grant No. DMR 1707565, ONR award N00014-20-1-2184, and Academy of Finland Grant No. 317141.

DATA AVAILABILITY STATEMENT

The data that support the findings of this study are available from the corresponding author upon reasonable request.

[1] W. B. Lynch, K. A. Earle, and J. H. Freed, Rev. Sci. Instrum. **59**, 1345 (1988).
[2] C. Caspers, P. F. da Silva, M. Soundararajan, M. A. Haider, and J.-P. Ansermet, APL Photon. **1**, 026101 (2016).
[3] W. Hofbauer, K. A. Earle, C. R. Dunnam, J. K. Moscicki, and J. H. Freed, Rev. of Sci. Instrum. **75**, 1194 (2004).
[4] S. Vasilyev, J. Järvinen, E. Tjukanoff, A. Kharitonov, and S. Jaakkola, Rev. Sci. Instrum. **75**, 94 (2004).
[5] J. Järvinen, J. Ahokas, S. Sheludiakov, O. Vainio, D. Zvezdov, L. Lehtonen, L. Vlasenko, and S. Vasiliev, Appl. Magn. Reson. **48**, 473 (2017).
[6] L. Bondorf, M. Beutel, M. Thiemann, M. Dressel, D. Bothner, J. Sichelschmidt, K. Kliemt, C. Krellner, and M. Scheffler, Physica B **536**, 331 (2018).

[7]P. Wang, K. Huang, J. Sun, J. Hu, H. Fu, and X. Lin, Rev. Sci. Instrum. **90**, 023905 (2019).
[8]J. Heckmann, S. Goertz, W. Meyer, E. Radtke, and G. Reicherz, Nucl. Instrum. Meth. A **526**, 110 (2004).
[9]S. Sheludiakov, J. Ahokas, O. Vainio, J. Järvinen, D. Zvezdov, S. Vasiliev, V. V. Khmelenko, S. Mao, and D. M. Lee, Rev. Sci. Instrum. **85**, 053902 (2014).
[10]V. Kiryukhin, E. P. Bernard, V. V. Khmelenko, R. E. Boltnev, N. V. Krainyukova, and D. M. Lee, Phys. Rev. Lett. **98**, 195506 (2007).
[11]S. Mao, A. Meraki, R. E. Boltnev, V. V. Khmelenko, and D. M. Lee, Phys. Rev. B **89**, 144301 (2014).
[12]J. Ahokas, J. Järvinen, V. V. Khmelenko, D. M. Lee, and S. Vasiliev, Phys. Rev. Lett. **97**, 095301 (2006).
[13]J. Ahokas, O. Vainio, S. Novotny, J. Järvinen, V. V. Khmelenko, D. M. Lee, and S. Vasiliev, Phys. Rev. B **81**, 104516 (2010).
[14]S. Sheludiakov, P. T. McColgan, D. M. Lee, V. V. Khmelenko, J. Järvinen, J. Ahokas, and S. Vasiliev, Phys. Rev. Lett. **122**, 225301 (2019).
[15]J. Ahokas, J. Järvinen, G. V. Shlyapnikov, and S. Vasiliev, Phys. Rev. Lett. **101**, 263003 (2008).
[16]S. Sheludiakov, J. Ahokas, J. Järvinen, D. Zvezdov, O. Vainio, L. Lehtonen, S. Vasiliev, S. Mao, V. V. Khmelenko, and D. M. Lee, Phys. Rev. Lett. **113**, 265303 (2014).
[17]`https://www.uhvdesign.com/`.
[18]https://www.attocube.com/en.
[19]http://www.krystaly.cz/en/.
[20]U. Albrecht, P. Evers, and P. Leiderer, Surf. Sci. **283**, 419 (1993).
[21]M. Sohaili, J. Klier, and P. Leiderer, J. Phys. Cond. Matter **17**, S415 (2005).
[22]A. Meraki, P. T. McColgan, R. E. Boltnev, D. M. Lee, and V. V. Khmelenko, J. Low Temp. Phys. **192**, 224 (2018).
[23]C. Poole, *Electron Spin Resonance: A Comprehensive Treatise on Experimental Techniques*, Dover books on physics (Dover Publications, 1996).
[24]J.-M. Spaeth, J. R. Niklas, and R. H. Bartram, *Structural Analysis of Point Defects in Solids*, Springer Series in Solid-State Sciences (Springer-Verlag Berlin Heidelberg, 1992).

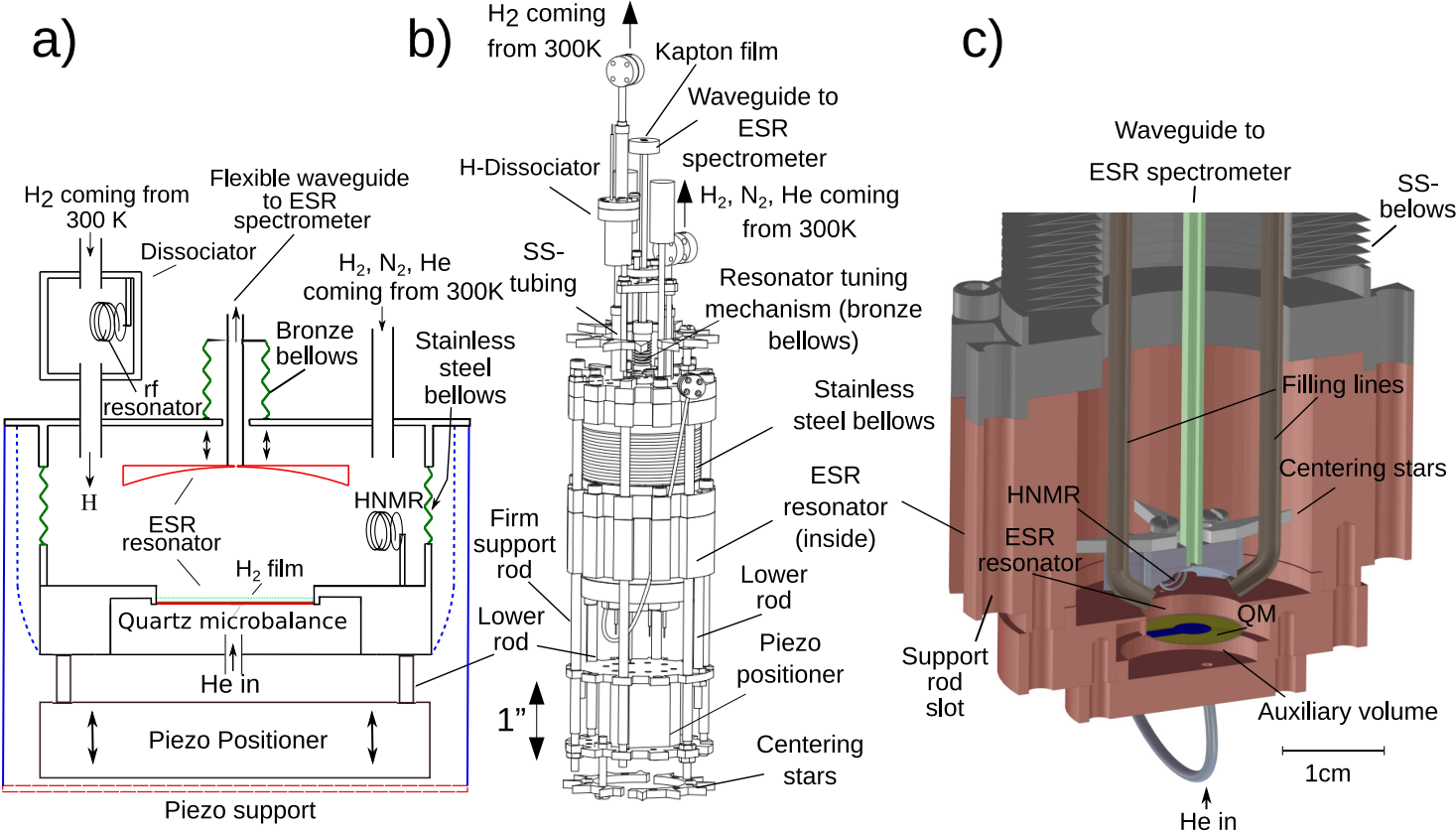
a)
H2 coming from 300 K
Flexible waveguide to ESR spectrometer
Dissociator
H2, N2, He coming from 300K
Bronze bellows
Stainless steel bellows
rf resonator
H
HNMR
ESR resonator
H2 film
Quartz microbalance
He in
Piezo Positioner
Piezo support
b)
H2 coming from 300K
Kapton film
Waveguide to ESR spectrometer
H-Dissociator
H2, N2, He coming from 300K
SS-tubing
Resonator tuning mechanism (bronze bellows)
Stainless steel bellows
ESR resonator (inside)
Firm support rod
Lower rod
Lower rod
Piezo positioner
1”
Centering stars
c)
Waveguide to ESR spectrometer
SS-belows
Filling lines
Centering stars
HNMR
ESR resonator
QM
Support rod slot
Auxiliary volume
1cm
He in

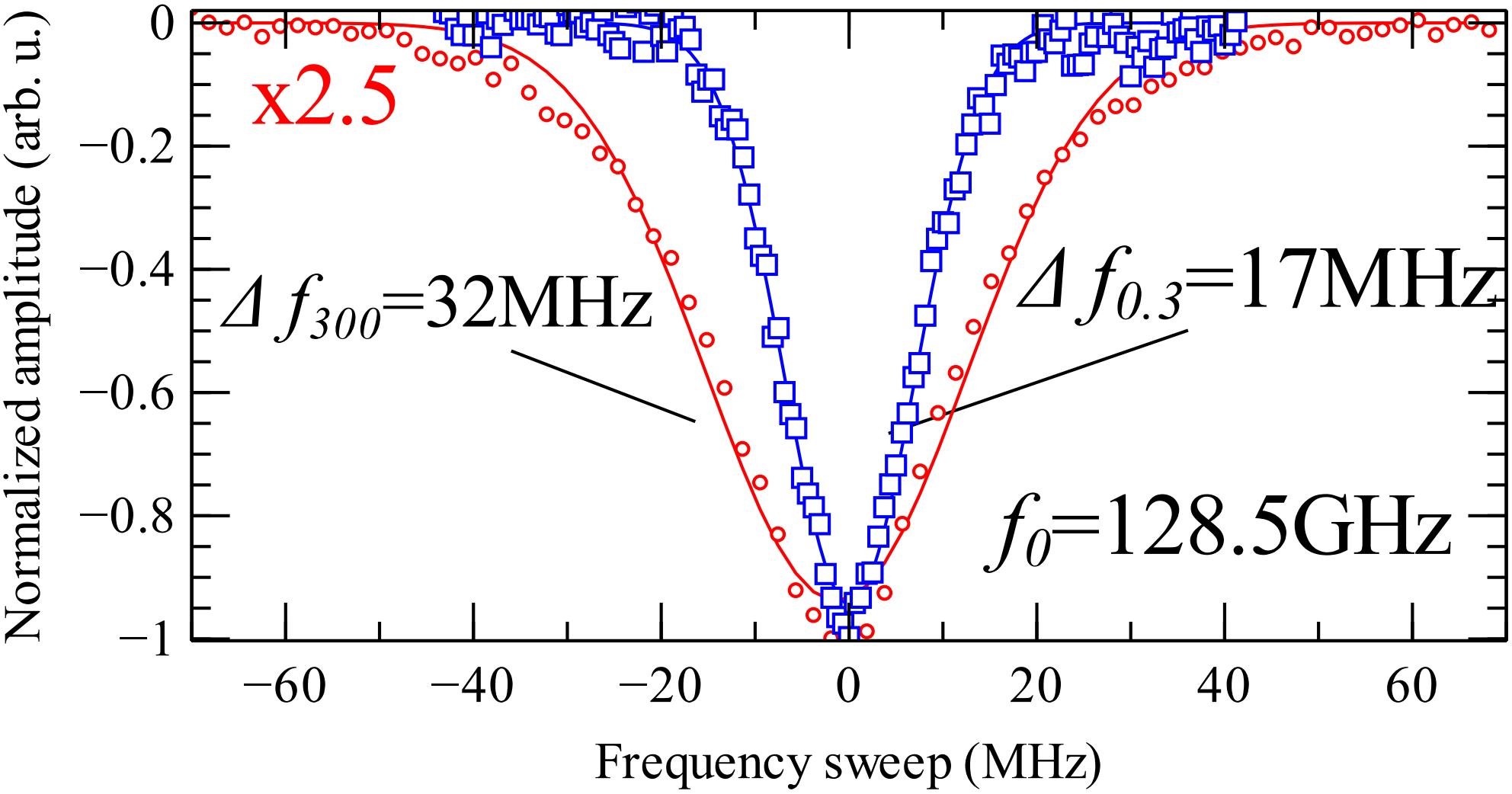
x2.5
Δf_{300}=32MHz
$\Delta f_{0.3}$=17MHz
f_0=128.5GHz
Normalized amplitude (arb. u.)
Frequency sweep (MHz)
0
−0.2
−0.4
−0.6
−0.8
−1
−60
−40
−20
0
20
40
60

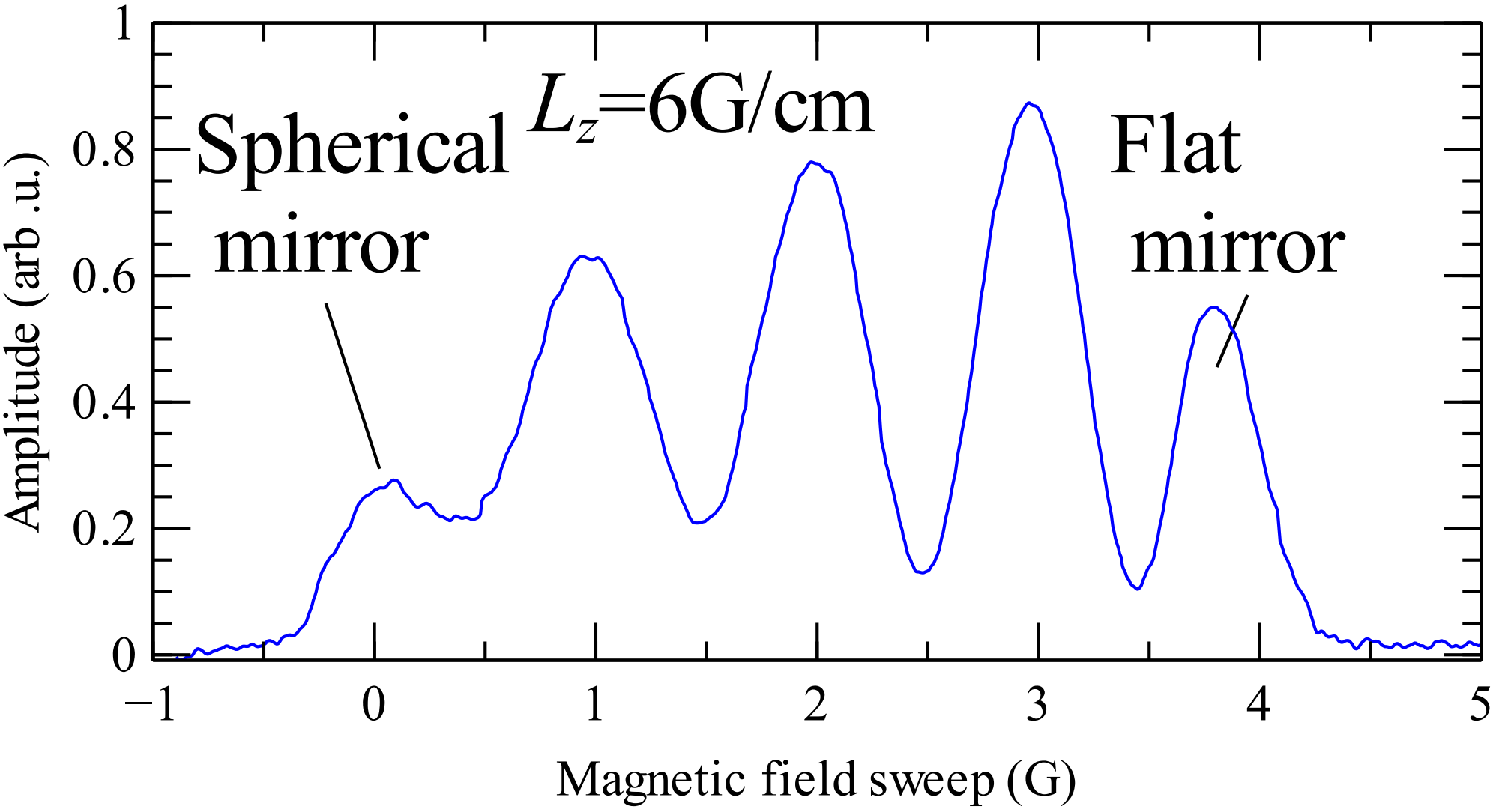
Spherical mirror
L_z=6G/cm
Flat mirror
Amplitude (arb .u.)
Magnetic field sweep (G)
1
0.8
0.6
0.4
0.2
0
−1
0
1
2
3
4
5

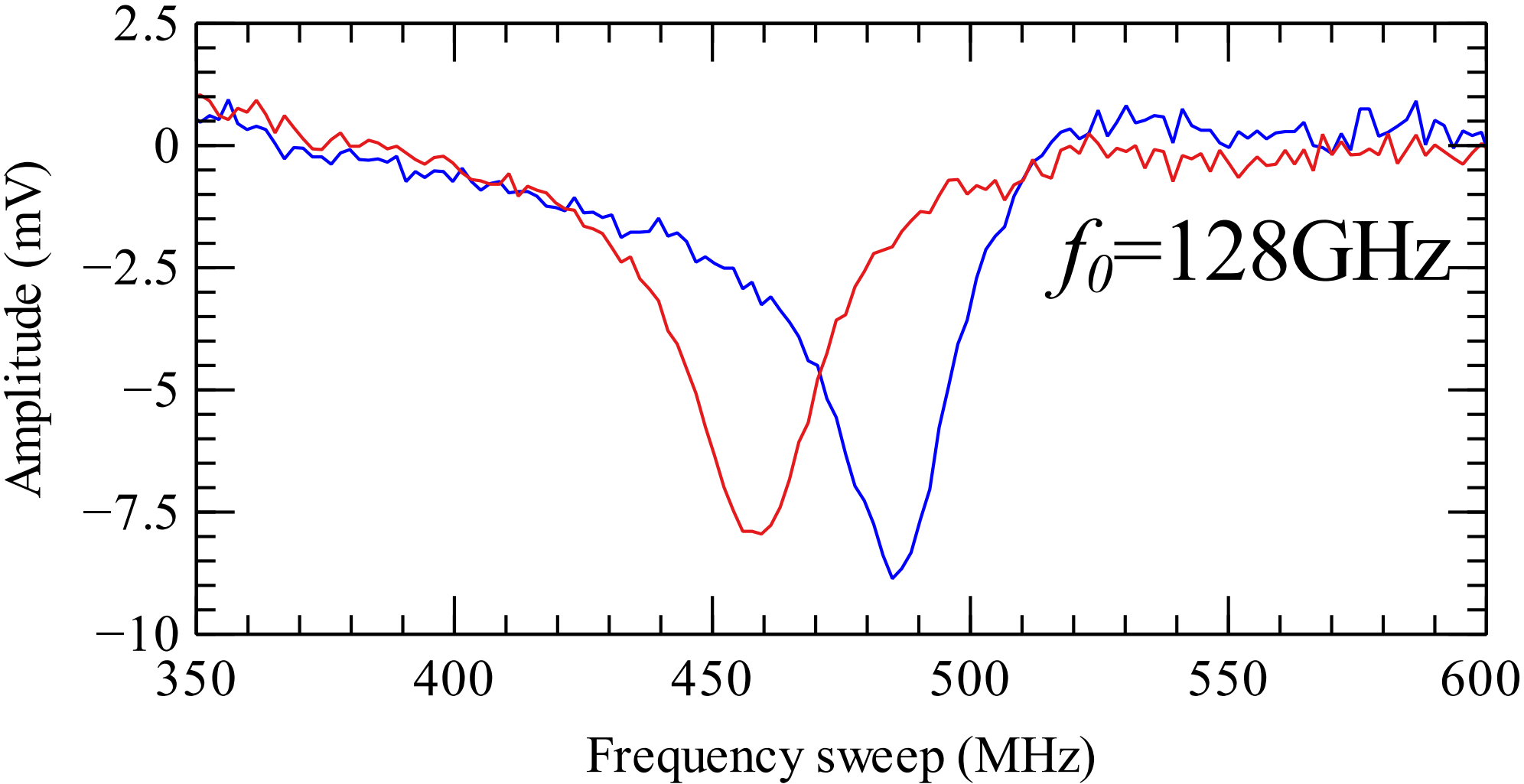
2.5
0
−2.5
−5
−7.5
−10
Amplitude (mV)
350
400
450
500
550
600
Frequency sweep (MHz)
f_0=128GHz

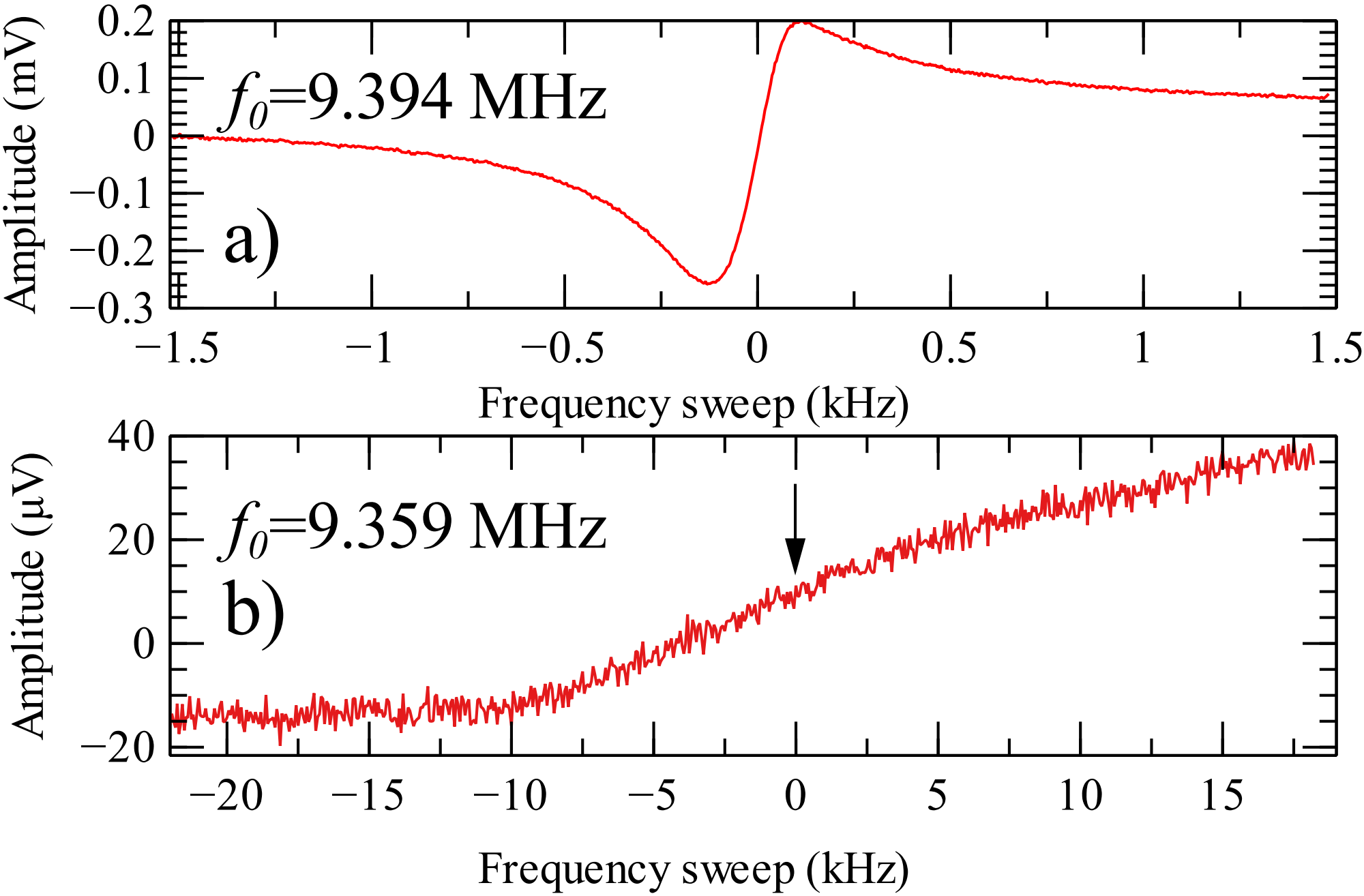
f_0=9.394 MHz
a)
Amplitude (mV)
0.2
0.1
0
−0.1
−0.2
−0.3
−1.5
−1
−0.5
0
0.5
1
1.5
Frequency sweep (kHz)
f_0=9.359 MHz
b)
Amplitude (μV)
40
20
0
−20
−20
−15
−10
−5
0
5
10
15
Frequency sweep (kHz)

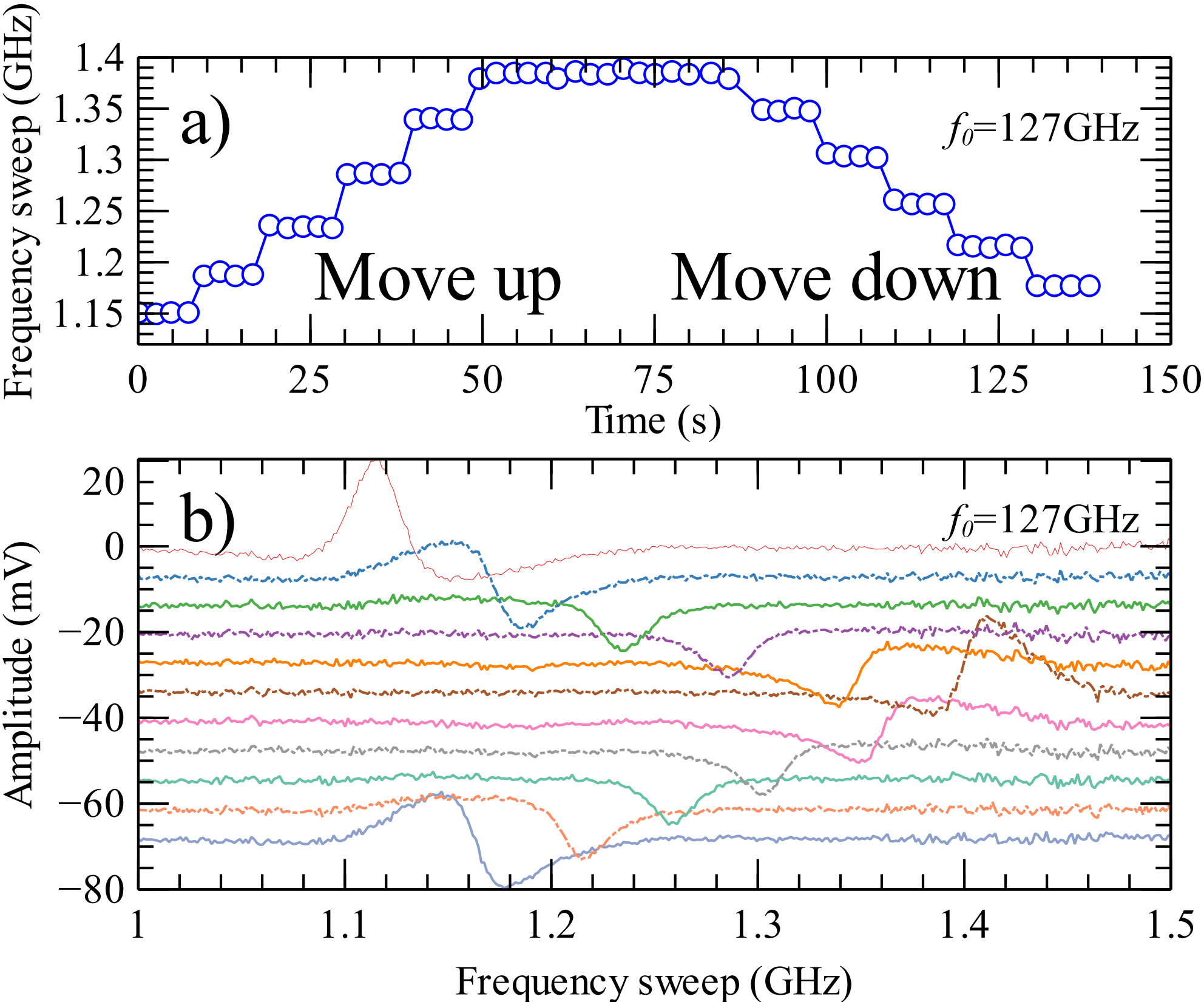
a)
f_0=127GHz
Move up
Move down
Frequency sweep (GHz)
Time (s)
b)
f_0=127GHz
Amplitude (mV)
Frequency sweep (GHz)

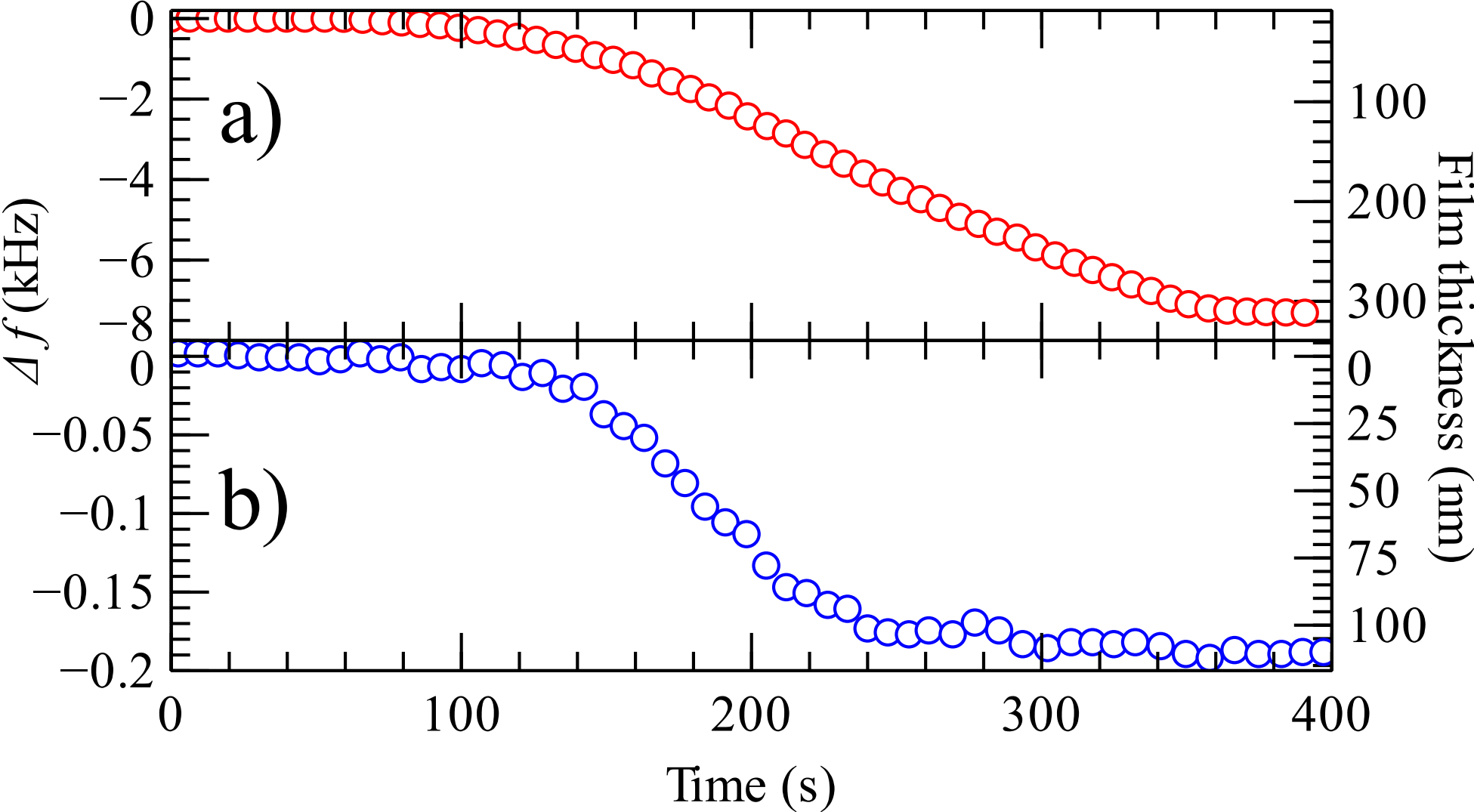
a)
b)
Δf (kHz)
Film thickness (nm)
Time (s)
0
−2
−4
−6
−8
0
−0.05
−0.1
−0.15
−0.2
100
200
300
0
25
50
75
100
0
100
200
300
400

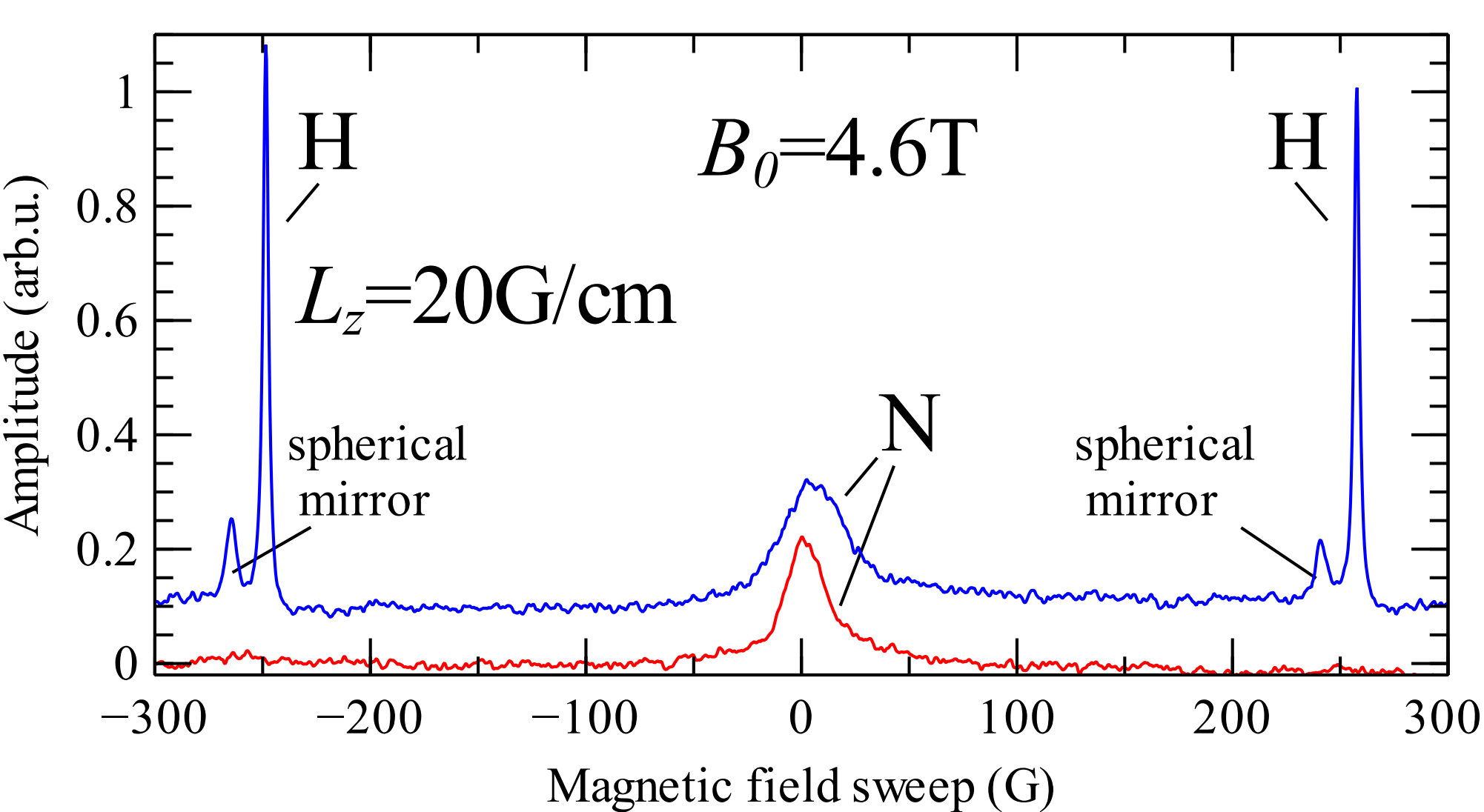
H
B_0=4.6T
H
L_z=20G/cm
N
spherical
mirror
spherical
mirror
Amplitude (arb.u.)
Magnetic field sweep (G)
1
0.8
0.6
0.4
0.2
0
−300
−200
−100
0
100
200
300

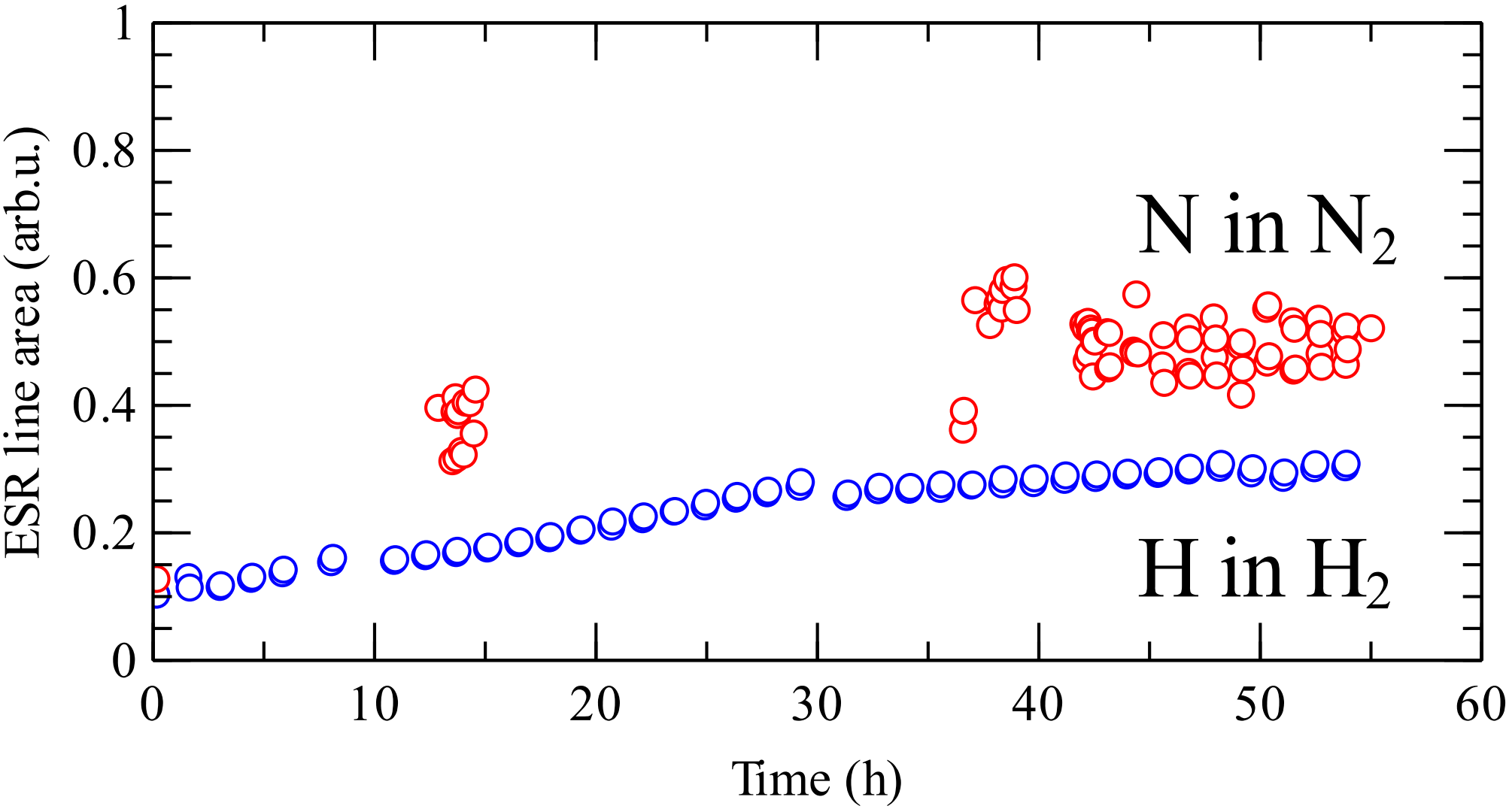
ESR line area (arb.u.)
Time (h)
N in N2
H in H2
0
0.2
0.4
0.6
0.8
1
0
10
20
30
40
50
60